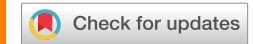
RESEARCH ARTICLE | OCTOBER 02 2020

Study on micromagnets induced local wavy mixing in a microfluidic channel **⊘**

Ran Zhou 🕶 📵 ; Athira N. Surendran 📵



Appl. Phys. Lett. 117, 132408 (2020) https://doi.org/10.1063/5.0024011





CrossMark

500 kHz or 8.5 GHz? And all the ranges in between.









Study on micromagnets induced local wavy mixing in a microfluidic channel

Cite as: Appl. Phys. Lett. **117**, 132408 (2020); doi: 10.1063/5.0024011 Submitted: 3 August 2020 · Accepted: 20 September 2020 · Published Online: 2 October 2020







Ran Zhou^{a)} (D) and Athira N. Surendran (D)

AFFILIATIONS

Department of Mechanical and Civil Engineering, Purdue University, Northwest. 2200 169th Street, Hammond, Indiana 46323, USA

^{a)}Author to whom correspondence should be addressed: zhou970@pnw.edu

ABSTRACT

The phenomenon of ferrofluid-water mixing is investigated using a double-layer magnetic micromixer, in which a layer of micromagnet bars is placed immediately below the fluid layer. A wavy pattern of the ferrofluid-water interface is surprisingly observed at each micromagnet responsible for improved mixing. The mechanism causing the wavy mixing is discovered and analyzed through experimental measurements and numerical simulations, and the mixing efficiency under different flow conditions is discussed. For flows with $Re \ll 1$, the resultant steep gradient of opposing magnetic forces by micromagnets in the ferrofluid region gives rise to a local pressure source that induces a transverse/spanwise pressure gradient and activates momentum transfer between fluids. The current finding enables effective localized mixing of ferrofluids with a small footprint and, thus, has great potential to achieve fast mixing for high-throughput flows with an integrated parallel system of multiple microfluidic channels and micromagnets.

Published under license by AIP Publishing. https://doi.org/10.1063/5.0024011

Microscale mixing is an essential step in many lab-on-chip and microfluidic systems, which are used in a wide range of applications such as chemical reaction processes, ^{1,2} biomedical diagnostics, ^{3,4} DNA analysis, ^{5,6} and polymer synthesis. ^{7,8} However, the Reynolds number for the flow in microfluidic channel is usually very small (Re < 1), and so the flow mixing mainly relies on weak laminar diffusion. Furthermore, the channel in these miniaturized devices is very short in length and the residence time is not long enough for fluids to achieve effective and homogeneous mixing. 9,10 Therefore, it is of great practical significance to realize rapid mixing in microfluidics given the nature of microscale laminar flow. The traditional working mechanisms of a micromixer rely on either complex design of the channel structure, 11-13 or the forces generated by external fields such as acoustic fields, ^{14–16} electrical fields, ^{17–19} and magnetic fields. ^{20–22} Among different methods, the integration of magnetic fields into a microfluidic device for rapid mixing exhibits advantages in biomedical/clinical applications concerning microscale biological objects (e.g., living cells) since the magnetic field provides an environment for cell viability. 9,22 Thus, the micro-mixing methodology using magnetic forces and ferrofluids has recently become a popular way to distribute nano magnetite particles (10 nm diameter suspended in ferrofluid) throughout biofluids with the target cells, so that only the bio-entities attached with nano magnetic particles will be isolated for subsequent analysis in the next stage.²⁴⁻²⁷ Different from the traditional micromixers using

electromagnets or bulky permanent magnets, ^{9,25,28,29} the micromagnets in this work produce zero Joule heat that harms the bio entities and can be fabricated and positioned with high precisions following the photo mask design with extra compactness achieved.

In this work, customized microscale magnets made of the neodymium powder and polydimethylsiloxane (NdFeB-PDMS) mixture were fabricated immediately underneath the microfluidic channel perpendicular to the streamwise direction to generate the magnetic field and realize rapid mixing between the superparamagnetic ferrofluid and water stream. The mixing process is captured using a high-speed camera and analyzed through image processing to quantify the mixing efficiency and fluid distributions. Surprisingly, a wavy pattern was observed to exist stably at the ferrofluid-water interface under the effect of the external magnetic field generated by NdFeB-PDMS micromagnets. Compared to our previous work with a "single-layer" micromixer design,²¹ the "double-layer" design with micromagnets placed directly underneath the fluidic channel significantly shortens the distance between ferrofluid and the magnet and, thus, strengthens the magnetic force exerted on ferrofluid, which also induces a different mechanism of momentum transfer to enhance the mixing efficiency.

Figure 1(a) shows the photograph of a double-layered micromixer with micromagnets fabricated and placed underneath the microfluidic channel. The channel is manufactured by an in-house developed soft lithography method, and so "double layers" refer to the

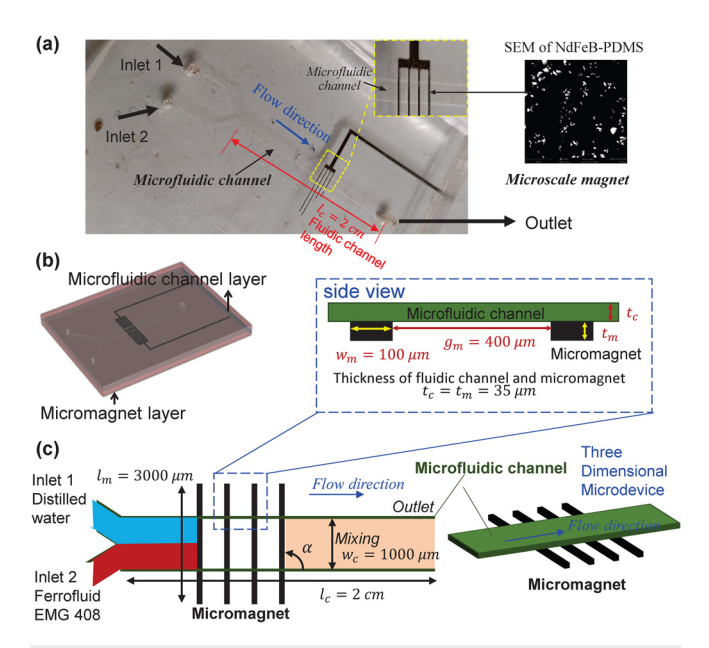


FIG. 1. (a) Photograph of the microfluidic device for rapid mixing. The smaller one is the SEM image of solidified NdFeB-PDMS. (b) computer-aided design (CAD) schematic of the device. (c) Dimension description of the micromixer. w_c and l_c are the width and length of the microfluidic channel, respectively; $\alpha=90^\circ$ is the angle between the micromagnet and the flow direction; l_m and w_m are the length and width of each micromagnet; g_m is the gap distance between each micromagnet; t_m and t_c are the thicknesses of the microfluidic channel and the micromagnet.

top microfluidic channel layer and the bottom micromagnet layer [Fig. 1(b)]. The Scanning Electron Microscope (SEM) image in Fig. 1(a) shows a uniform texture of a solidified NdFeB–PDMS micromagnet. In Fig. 1(c), the distilled water and ferrofluid with an original magnetic nanoparticle concentration of 1.2% (v/v) (EMG 408, Ferrotec) are injected into the microfluidic channel from Inlet 1 and Inlet 2, respectively, with a sharp interface between fluids before mixing starts at the four micromagnets. The thicknesses of both the micromagnet (t_m) and the microfluidic channel (t_c) are 35 μ m, the same as the dry photoresist film thickness (MM540, DuPont). In the experiment, the inlet flow rates are controlled by two syringe pumps separately (74900, Cole-Parmer). The micromixer was placed on an inverted microscope stage (IN 300TC-FL, Amscope), and mixing videos are recorded using a high-speed camera (AX 200, Photon).

The in-house low-cost soft lithography fabrication process³⁰ of the double-layer magnetic micromixer is demonstrated in Fig. 2. First, a dry film photoresist was laminated [Fig. 2(b)] onto a copper plate [Fig. 2(a)]. With ultra-violet (UV) exposure [Fig. 2(c)] through a transparency photo mask (10 000 dpi, CAD/Art Services), the exposed dry film was developed, rinsed, and dried to obtain the master mold [Fig. 2(d)]. PDMS was cast on the master mold [Fig. 2(e)]. After curing, the PDMS replica was peeled off and boned to a glass slide [Fig. 2(f)]. Then, the NdFeB–PDMS mixture was injected into the hollow structure [Fig. 2(g)] and solidified to form a magnetic bar on a hotplate at 120 °C, which was magnetized using an impulse magnetizer (IM 10, ASC Scientific) to become a permanent micromagnet. Finally, the micromagnet layer was bonded with prefabricated microfluidic channel layer PDMS by corona surface treatment [Fig. 2(h)].

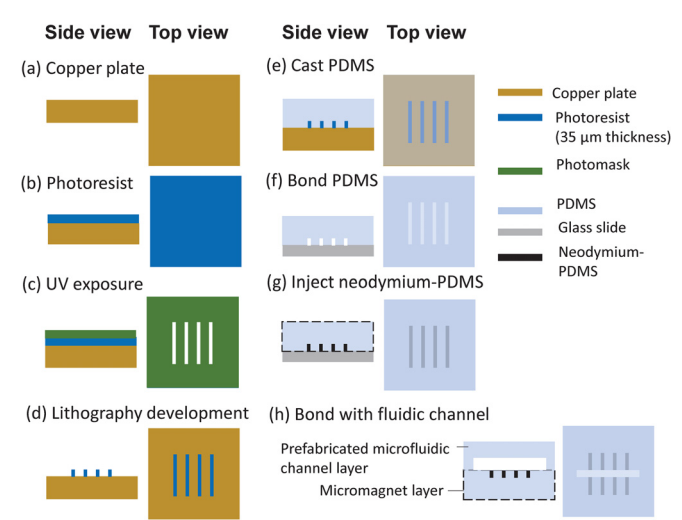


FIG. 2. Fabrication steps of the micromixer (see the supplementary material). (a) Preparation of the substrate. (b)–(d) Bonding, exposure, and fabrication of photoresist. (e) Casting of PDMS to copper mold. (f) and (g) Bonding of PDMS and injecting the magnetic mixture. (h) Bonding of the magnet layer with the channel layer.

A close-up observation of the ferrofluid motion under the effect of the NdFeB-PDMS magnet is performed in the area within a window of $l = 4500 \,\mu\text{m}$ near the micromagnets [Fig. 3(a)]. Figures 3(b1)-3(b6) show experimental ferrofluid mixing at different total flow rates ranging from Q = 0.04 ml/h to Q = 4.5 ml/h. The flow rate ratio between water and ferrofluid is fixed constant at 1:1 for all experiments, and so the distributed widths of each flow stream are kept the same at the inlet. At a lower total flow rate [Q = 0.04-0.1 ml/h, Figs.]3(b1) and 3(b2)], the sharp interface between water and ferrofluid disappeared as flow passed the four vertical micromagnets, indicating enhanced mixing between the distilled water and ferrofluid under the magnetic field by the microscale magnets; while at higher flow rates, the interface only turned blurry at the outlet. Compared to the total flow rate of Q = 4.5 ml/h [Fig. 3(b6)], mixing is more complete and more homogeneous at $Q = 0.04 \,\text{ml/h}$ [Fig. 3(b1)] because the residence time of ferrofluid is longer for magnetic force to act on it when flow velocity is slower.

Surprisingly, a wavy pattern of the water–ferrofluid interface is visually identified at each micromagnet when the flow rate is relatively low, e.g., at $Q = 0.04 \, \text{ml/h}$ [Fig. 3(b1)], $Q = 0.1 \, \text{ml/h}$ [Fig. 3(b2)], and $Q = 0.2 \, \text{ml/h}$ [Fig. 3(b3)]. This interesting phenomenon is clearly related to the externally imposed magnetic field through observation and could be a hinted mechanism causing ferrofluid mixing. To confirm this hypothesis, a 2D multiphysics model was developed in COMSOL® to explore this hidden physics and reveal the details of ferrofluids passing the magnetic field. In the numerical model, both distilled water and ferrofluids are considered as incompressible fluids of different species, and so the Navier–Stokes and continuity equations are solved to obtain momentum and mass conservations of the transient flow in the microfluidic channel,

$$\rho \frac{\partial \mathbf{u}}{\partial t} + \rho (\mathbf{u} \cdot \nabla) \mathbf{u} = -\nabla p + \eta \nabla^2 \mathbf{u} + \mathbf{f_m}, \tag{1}$$

$$\nabla \cdot \mathbf{u} = 0, \tag{2}$$

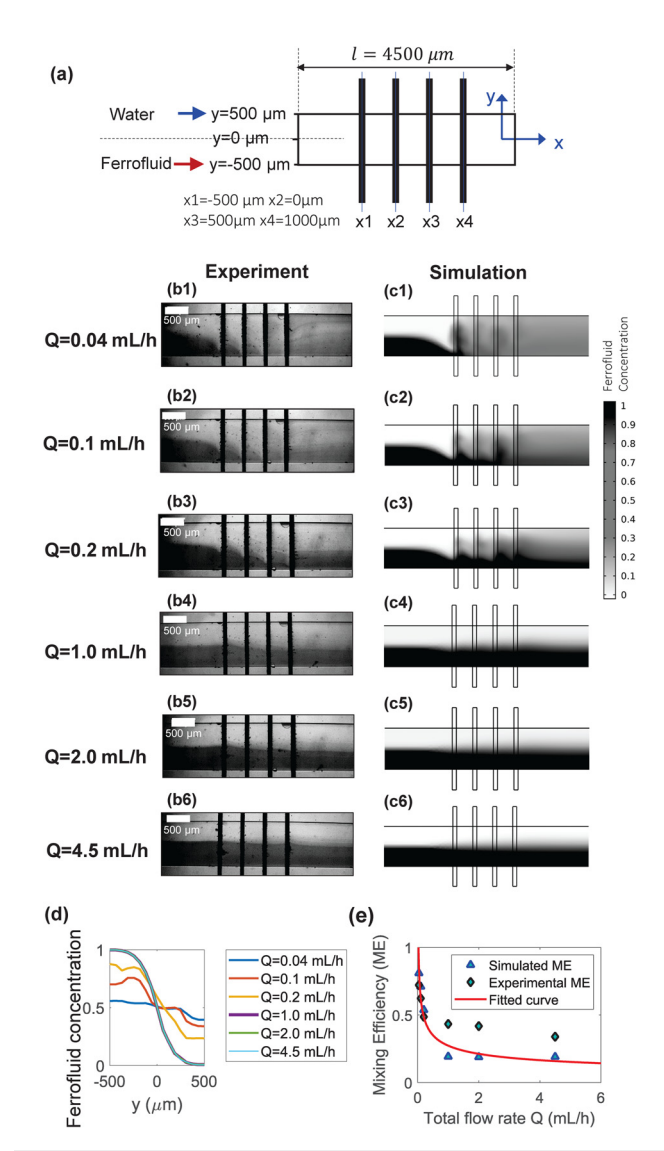


FIG. 3. (a) Schematic and dimension of the close-up view around the micromagnet. (b) and (c) show the experiment measured and simulation predicted ferrofluid distributions in the microfluidic channel under the effect of the magnetic field by the four micromagnet bars with the total flow rate Q varying from 0.04 ml/h to 4.5 ml/h. The flow rate ratio between ferrofluid and distilled water is 1:1 for all the groups. (d) shows the extracted ferrofluid concentration profiles from group (c) along y $=-500~\mu{\rm m}$ to y $=500~\mu{\rm m}$. (e) Experimental and simulated mixing efficiencies corresponding to groups (b) and (c).

where ρ is the fluid mixture density, ${\bf u}$ is the fluid velocity, p refers to the pressure, η denotes the dynamic viscosity, and ${\bf f_m}$ is the magnetic force per unit volume. Note that during the mixing process, the density and viscosity of the mixture vary with the local ferrofluid concentration $\rho = c\rho_f + (1-c)\rho_w$ and $\eta = \eta_f e^{R(1-c)}$, where c is the species concentration, R is a viscosity parameter, and $R = \ln(\eta_w/\eta_f)$. ρ_f , ρ_w , η_f and η_w represent the density and viscosity of pure ferrofluid and distilled water, respectively. The Considering mass fluxes by diffusion and convection, the resulting mass balance is $\nabla \cdot (-D\nabla c + c{\bf u}) = 0$,

where D denoting the mass diffusion coefficient of ferrofluid is $3.6 \times 10^{-14} \text{ m}^2/\text{s}$ at room temperature.

The magnetic force f_m is the key factor to couple the external magnetic field and ferrofluid motion that leads to mixing behavior, and so here, it is discussed in detail. In the presence of a magnetic field gradient, the nanomagnetic particles experience a magnetic force, which can be modeled using a dipole moment approach by replacing the magnetized particle with an "equivalent" point dipole. 32 In this way, the magnetic body force density acting on the miscible ferrofluid mixture is $\mathbf{f}_m = \mu_0(\mathbf{M} \cdot \nabla)\mathbf{H}$, where $\mu_0 = 4\pi \times 10^{-7}$ H/m is the magnetic permeability of free space, M is the field-dependent magnetization of the miscible ferrofluid mixture, which is proportional to the magnetization of the original ferrofluid M_0 , with $M = M_0 c$, and H is the external applied magnetic field with a magnitude of 11 000 A/m. When the magnetization is aligned with the applied magnetic field H, M_0 is modeled as $M_0 = \chi H$, where $\chi = 0.5$ is the magnetic susceptibility of ferrofluid.³¹ Therefore, the magnetic force acting on ferrofluid per unit volume can be expressed as

$$\mathbf{f_m} = \mu_0 c \chi(\mathbf{H} \cdot \nabla) \mathbf{H}. \tag{3}$$

In the current multiphysics model, the magnetic field is obtained through a separate magnetization sub-model that solves for the magnetic field distributions to achieve the coupling with fluid flow simulations. Figures 3(c1)-3(c6) show the simulation results using the above numerical scheme and indicate very good agreement with experiments in Fig. 3(b), confirming the reasonable explanation in Eqs. (1)-(3). Ferrofluid concentration profiles along the transverse y-direction at the outlet of the microfluidic channel were extracted from Figs. 3(c1)-3(c6) and are plotted in Fig. 3(d). It is apparent that the ferrofluid concentration distribution of Q = 0.04 ml/h is very uniform and close to c = 0.5, indicating that the mixing is almost complete. As the total flow rate increases, the ferrofluid concentration profiles become steeper, confirming that the mixing between ferrofluid and distilled water is weaker. When the total flow rate is equal to or greater than Q = 1.0 ml/h, the ferrofluid concentration distributions are close to each other because little mixing occurred before fluids reached the channel outlet due to higher momentum and shorter residence time of the moving ferrofluid in the channel for the magnetic force to act on. The mixing efficiency in Eq. (4) of both experiment and simulation results in Figs. 3(a) and 3(b) is listed in Fig. 3(e). We used an in-house MATLAB code to evaluate the image intensity and obtain the mixing efficiency,3

$$ME = 1 - \sqrt{1/N \sum_{i=1}^{n} \left(\frac{I_i^* - \overline{I^*}}{\overline{I^*}}\right)^2},$$
 (4)

where $I^* = \frac{I - I_{\min}}{I_{\max} - I_{\min}}$ is the normalized intensity and I, I_{\max} and I_{\min} are the local, maximum, and minimum pixel intensities in the cropped image. $\overline{I^*}$ is the mean value of normalized intensities in the region of interest. The mixing efficiency of ME = 0 and ME = 1 indicates no mixing and full mixing, respectively. In Fig. 3(e), it is evident that as the flow rate increased, the mixing efficiency decreased and approached zero when the flow rate is fast enough. The difference between experiment and simulation is caused by the background noise of real light source brightness.

To explain the water-ferrofluid mixing and the wavy pattern of the ferrofluid concentration profile between micromagnets, the

experiment in Fig. 3(b3) when the total flow rate Q = 0.2 ml/h is analyzed as an example. It is shown in Fig. 4(a) that the forces are negligible in regions away from the micromagnets as well as in the upper half of the channel where the ferrofluid concentration is zero. It is also worth noting that the body forces are concentrated in regions close to the vertical boundaries of each micromagnet, mostly parallel to the streamwise direction but opposite to each other at the pair of the vertical boundaries of each micromagnet. Thus, in fact, it is f_{mx} that dominates the ferrofluid mixing (see the supplementary material for force analysis). According to Eq. (3), f_{mx} is proportional to $(H_x \frac{\partial H_x}{\partial x} + H_y \frac{\partial H_x}{\partial y})$ in Fig. 4(b), which only highlights the two vertical zones close to the pair of boundaries for each micromagnet. This is also consistent with the magnetic force distribution. When ferrofluid approaches the left-side boundary of a micromagnet, the magnetic force points to (roughly) the streamwise direction, which accelerates the ferrofluid flow [Fig. 4(c)], and therefore, the flow area (or width seen from 2D) of the ferrofluid becomes narrower at a constant flow rate. On the contrary, when ferrofluid passes the micromagnets, the direction of magnetic force is flipped and becomes opposite with the streamwise direction causing deceleration of the flow. This resistance of flow momentum caused by the magnetic field and gradient abruptly reduces the ferrofluid streamwise velocities near the right-side vertical boundary of the micromagnet, which, in turn, widens the flow area (width in 2D) of the ferrofluid under the constant flow rate condition. Meanwhile, the sudden acceleration and deceleration of the ferrofluid streamwise velocity create a local pressure buildup, which leads to a transverse pressure gradient across the width of the channel, as demonstrated in Figs. 4(d) and 4(e), and so the pressure is higher in the lower half occupied with ferrofluid than that in the top half with distilled water. According to the momentum equation, this pressure difference in the transverse direction across the channel width induces an upward momentum pushing the ferrofluid toward the upper channel region where distilled water resides. Combining these two effects, with the mass conservation of ferrofluid and the transverse pressure gradient across the channel width, the mixing between ferrofluid and water is significantly enhanced. To quantitatively analyze the pressure distribution effect on mixing, the following pressure Poisson equation is derived by taking divergence at both sides of Eq. (1):

$$\nabla^2 p = \nabla \cdot \mathbf{f_m} - \rho \nabla \cdot [(\mathbf{u} \cdot \nabla)\mathbf{u}]. \tag{5}$$

When the total flow rate is small (Q = 0.04–0.2 ml/h, Re = 0.043–0.22), (1) the divergence of advection term $-\nabla \cdot [(\boldsymbol{u} \cdot \nabla)\boldsymbol{u}]$ is very small compared to the magnetic body force gradient and can be neglected and (2) the magnetic body force gradient in the streamwise direction at micromagnets $\frac{\partial f_{mx}}{\partial x}$ dictates $\nabla \cdot \mathbf{f_m}$ and is much smaller than 0 (see the supplementary material for a detailed derivation). Thus, it is important to find that the inequality holds for pressure of ferrofluid in the bottom channel region when Re \ll 1,

$$\nabla^2 p \ll 0. \tag{6}$$

Intuitively, inequality six suggests that a "pressure source" is present in the ferrofluid within the width of the micromagnet, which gives rise to a spanwise pressure gradient as confirmed by the numerical simulation results under low throughput conditions (Re \ll 1) as shown in Fig. 4(e). To explore the flow rate effect on mixing, a parameter, dp_{trans}/p_c , is defined to characterize the relative significance of the transverse momentum transfer compared to flow momentum in the streamwise direction, where dp_{trans} represents the pressure difference in the transverse direction induced by the micromagnets, $p_c = 1/2\rho U^2$, and U is the superficial velocity. In Fig. 4(f), dp_{trans}/p_c is plotted for each micromagnet against different channel flow rates. It is evident that the transverse momentum transfer is more significant when a small flow rate is present. When the channel flow rate is higher

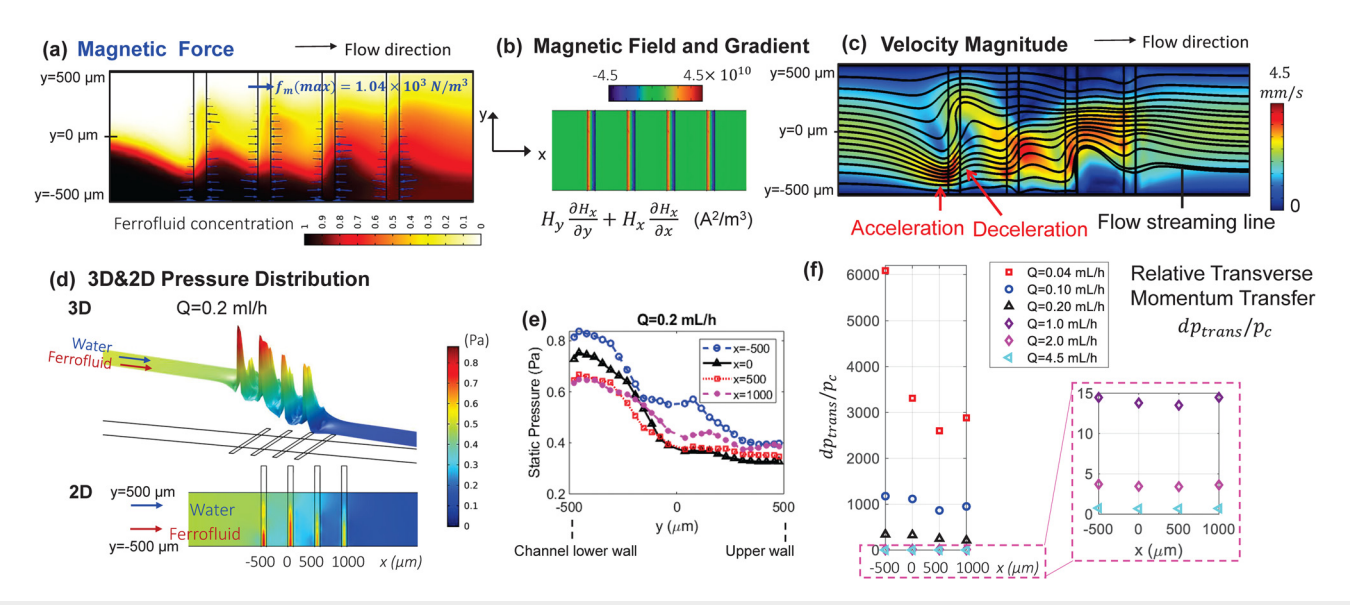


FIG. 4. (a) Ferrofluid concentration distribution near the micromagnet and magnetic force f_m acting on ferrofluid. (b) Magnetic field and its gradient generated by the micromagnet. (c) Flow streaming line and velocity magnitude distribution in the microfluidic channel. (d) and (e) Pressure distribution inside the microfluidic channel. (a)–(e) correspond to the experiment in Fig. 3(b3) when the total flow rate $Q = 0.2 \, \text{ml/h}$. The coordinate in (a)–(e) is referred to Fig. 3(a). (f) shows the relative transverse momentum transfer at each micromagnet at different total flow rates.

than 1.0 ml/h corresponding to a dp_{trans}/p_c value of 15, the mixing of ferrofluid and distilled water is no longer pronounced, and the wavy pattern of ferrofluid concentration distribution is not obvious and fades out. This observation is consistent with the measured experimental mixing performance as shown in Fig. 3(b).

In this Letter, an interesting phenomenon of ferrofluid mixing in a double-layer micromixer with embedded micromagnets is studied. A wavy pattern of ferrofluid concentration distribution is observed at the ferrofluid-water interface between micromagnets responsible for the mixing enhancement. The numerical simulations show that the magnetic volume force generated by each micromagnet causes ferrofluid to accelerate and immediately decelerate within a short distance of the width of the micromagnet bar, which tends to narrow and expand the ferrofluid flow passage and distort the ferrofluid-water interface. More importantly, combining experiment measurements and numerical simulations, a local pressure source in the ferrofluid layer is identified through Poisson inequality $\nabla^2 p \ll 0$ when flow passes the micromagnet that leads to a unique transverse pressure difference and contributes to the momentum transfer in the channel spanwise direction. As a result, a more homogeneous mixing between ferrofluid and water is achieved under low-throughput conditions with a high dp_{trans}/p_c number. This work is of great significance to be noted in the study of rapid mixing at the microscale at low flow rates. The double-layer micromixer developed in the current work can be applied in a number of clinical and biological applications that require ample premixing of fluid samples, for instance, to tag target cells in the biofluid with magnetic particles, which will later be separated from contaminated blood for further diagnosis, to help with synthesis of protein, and as a microreactor for enzyme processing.

See the supplementary material for the analysis of the magnetic force-induced spanwise pressure gradient in the microchannel and fabrication details of the double-layer micromixer.

DATA AVAILABILITY

The data that support the findings of this study are available from the corresponding author upon reasonable request.

REFERENCES

- ¹P. Plouffe, D. M. Roberge, and A. Macchi, Chem. Eng. J. 300, 9 (2016).
- ²Y. Zhang, M. Sesen, A. de Marco, and A. Neild, Anal. Chem. 92, 10725 (2020).
- ³Y. Zhao, D. Xu, and W. Tan, Integr. Biol. 9, 188 (2017).
- ⁴X. Su, Y. Xu, H. Zhao, S. Li, and L. Chen, Talanta 194, 903 (2019).

- ⁵A. S. Kastania, K. Tsougeni, G. Papadakis, E. Gizeli, G. Kokkoris, A. Tserepi, and E. Gogolides, Anal. Chim. Acta 942, 58 (2016).
- ⁶I. Hernández-Neuta, I. Pereiro, A. Ahlford, D. Ferraro, Q. Zhang, J.-L. Viovy, S. Descroix, and M. Nilsson, Biosens. Bioelectron. 102, 531 (2018).
- ⁷D. Wilms, J. Klos, and H. Frey, Macromol. Chem. Phys. 209, 343 (2008).
- ⁸Y. Liu and X. Jiang, Lab Chip 17, 3960 (2017).
- ⁹M. Hejazian and N.-T. Nguyen, Micromachines 8, 37 (2017).
- ¹⁰G. Cai, L. Xue, H. Zhang, and J. Lin, Micromachines 8, 274 (2017).
- ¹¹D. J. Beebe, R. J. Adrian, M. G. Olsen, M. A. Stremler, H. Aref, and B.-H. Jo, Méc. Ind. 2, 343 (2001).
- ¹²B. Hama, G. Mahajan, P. S. Fodor, M. Kaufman, and C. R. Kothapalli, Microfluid. Nanofluid. 22, 54 (2018).
- ¹³C. Chen, Y. Zhao, J. Wang, P. Zhu, Y. Tian, M. Xu, L. Wang, and X. Huang, Micromachines 9, 160 (2018).
- Micromachines 9, 160 (2018).

 14.T. Frommelt, M. Kostur, M. Wenzel-Schäfer, P. Talkner, P. Hänggi, and A.
- Wixforth, Phys. Rev. Lett. 100(3), 034502 (2008).
 15 W. Cui, H. Zhang, H. Zhang, Y. Yang, M. He, H. Qu, W. Pang, D. Zhang, and X. Duan, Appl. Phys. Lett. 109, 253503 (2016).
- ¹⁶H. Chen, C. Chen, S. Bai, Y. Gao, G. Metcalfe, W. Cheng, and Y. Zhu, Nanoscale 10, 20196 (2018).
- ¹⁷C. Chang and R. Yang, Microfluid. Nanofluid. 3(5), 501 (2007).
- ¹⁸Y. Guan, F. Xu, B. Sun, X. Meng, Y. Liu, and M. Bai, Biomed. Microdevices 22(3), 47 (2020).
- ¹⁹ A. Kothandaraman, Y. Alfadhl, M. Qureshi, M. Edirisinghe, and Y. Ventikos, Langmuir 35, 10052 (2019).
- ²⁰L. Lu, K. Ryu, and C. Liu, J. Microelectromech. Syst. 11(5), 462 (2002).
- ²¹R. Zhou, A. N. Surendran, M. Mejulu, and Y. Lin, Micromachines 11, 29 (2019).
- ²²G. Chen, B. Ji, Y. Gao, C. Wang, J. Wu, B. Zhou, and W. Wen, Sens. Actuators, B 286, 181 (2019).
- ²³M. Hejazian and N.-T. Nguyen, Lab Chip **15**, 2998 (2015).
- ²⁴M. Zolgharni, S. M. Azimi, M. R. Bahmanyar, and W. Balachandran, Microfluid. Nanofluid. 3, 677 (2007).
- ²⁵D. Nouri, A. Zabihi-Hesari, and M. Passandideh-Fard, Sens. Actuators, A 255, 79 (2017).
- ²⁶G. Kitenbergs, K. Erglis, R. Perzynski, and A. Cēbers, J. Magn. Magn. Mater. 380, 227 (2015).
- ²⁷M. Ballard, D. Owen, Z. G. Mills, P. J. Hesketh, and A. Alexeev, Microfluid. Nanofluid. 20, 88 (2016).
- ²⁸C.-Y. Wen, C.-P. Yeh, C.-H. Tsai, and L.-M. Fu, Electrophoresis 30, 4179 (2009).
- ²⁹N. Kim, W. X. Chan, S. H. Ng, Y.-J. Yoon, and J. B. Allen, Micromachines 11, 636 (2020).
- 30 Z. Zhang, R. Zhou, D. Brames, and C. Wang, Micro Nanosyst. 7, 4 (2015).
- ³¹C.-Y. Wen, K.-P. Liang, H. Chen, and L.-M. Fu, Electrophoresis 32, 3268 (2011).
- ³²E. P. Furlani, Materials 3, 2412 (2010).
- ³³Z. Wu, N.-T. Nguyen, and X. Huang, J. Micromech. Microeng. 14, 604 (2004).
- 34T.-H. Tsai, D.-S. Liou, L.-S. Kuo, and P.-H. Chen, Sens. Actuators, A 153, 267 (2009).